Time-resolved relaxation dynamics of Hg_n^- $(11 \leqslant n \leqslant 16, n=18)$ clusters following intraband excitation at 1.5 eV

Jan R. R. Verlet, Arthur E. Bragg, and Aster Kammrath
Department of Chemistry, University of California, Berkeley, California 94720

Ori Cheshnovsky
School of Chemistry, Sackler Faculty of Exact Sciences, Tel-Aviv University, 69978 Israel

Daniel M. Neumark[a)]
Department of Chemistry, University of California, Berkeley, California 94720
and Chemical Sciences Division, Lawrence Berkeley National Laboratories, California 94720

(Received 6 August 2004; accepted 2 September 2004)

Electron-nuclear relaxation dynamics are studied in Hg_n^- $(11 \leqslant n \leqslant 16, n=18)$ using time-resolved photoelectron imaging. The excess electron in the anion uniquely occupies the *p* band and is excited intraband by 1.53 eV pump photons; the subsequent dynamics are monitored by photodetachment at 3.06 eV and measurement of the photoelectron images as a function of pump-probe delay. The initially excited state decays on a time scale of ~10 ps, and subsequent relaxation dynamics reveal a smooth evolution of the photoelectron spectra towards lower electron kinetic energy over 50–100 ps. Qualitatively, the relaxation process is captured by a simple kinetic model assuming a series of radiationless transitions within a dense manifold of electronic states. All the clusters studied show similar dynamics with the exception of Hg_{11}^- in which the initially prepared state does not decay as quickly as the others. © *2004 American Institute of Physics.* [DOI: 10.1063/1.1809573]

I. INTRODUCTION

Ultrafast dynamics in molecules and in condensed phases have been studied intensely over the last two decades.[1,2] Clusters have also received considerable attention, as their size-dependent properties address the gap between the discrete nature of isolated atoms or molecules and the continuous band structure associated with the condensed phase.[3–5] For large metallic aggregates, dynamics are reflective of the bulk with perturbations due to quantum confinement and the large fraction of surface atoms. However, even very small metal clusters can reveal properties and dynamics normally associated with extended systems. Alkali metal clusters such as Na_n with fewer than ten atoms have been shown to exhibit collective plasmon excitations in their electronic absorption spectra.[6] Photoelectron spectroscopy (PES) of transition metal cluster anions such as V_n^- clusters show signatures of the bulk electronic band structure beginning in the range $13 \leqslant n \leqslant 17$.[7] Manifestations of bulk phenomena are also seen in the dynamics of small transition metal clusters. Ultrafast electronic relaxation dynamics on time scales of tens of femtoseconds have been observed in transition metal clusters with as few as three atoms using time-resolved PES and are attributed to electron-electron scattering, a phenomena normally associated with bulk metals.[8–13] In contrast, electronic structure in Hg_n clusters evolves over a much larger size range, with cluster sizes in the range of $n=400$ required before band structure characteristic of a metal is observed,[14] while results for much smaller anion clusters suggested the presence of electron-hole recombination and Auger decay subsequent to electronic excitation.[15] These intriguing results motivate the work described here in which the electronic relaxation dynamics of size-selected Hg_n^- are investigated with time-resolved photoelectron imaging.

The evolution of electronic structure with size in Hg_n clusters has attracted considerable interest. The Hg atom has a closed shell configuration, $5d^{10}6s^2$, and its dimer forms a van der Waals molecule, bound by only 70 meV.[16] Further aggregation forms Hg_n clusters where the *s* states evolve into a filled *s* band, containing $2n$ electrons, whereas the higher-lying *p* states form an empty *p* band. However, as more atoms are added to the cluster, hybridization of the *s*-type orbitals with the *p*-type orbitals causes covalent character to be established in the bond. There is a body of experimental[17–21] and theoretical[22,23] work indicating that the transition from van der Waals to covalent bonding occurs in the range of $13 \leqslant n \leqslant 20$ atoms. Clusters larger than this are much like a semiconductor with a band gap separating the valence and conduction bands.

Upon further aggregation, Hg_n undergoes a nonmetal to metal transition as the full *s* band merges with the empty *p* band. Photoelectron-photoion coincidence measurements on neutral Hg_n suggest that clusters as small as $n=60$ exhibit electronic structure characteristic of bulk metals.[24] More direct insight into this issue was provided by negative ion PES experiments on Hg_n^- clusters by Busani, Folkers, and Cheshnovsky,[14] in which the extra electron uniquely occupies the bottom of the *p* band, corresponding to the lowest unoccupied molecular orbital (LUMO) of the neutral. The PE spectra of these clusters show a peak corresponding to detachment of this *p* electron, which is well separated from the broad detachment of the *s*-band electrons. The gap be-

[a)]Electronic mail: dan@radon.cchem.berkeley.edu

tween the two reflects the band gap of the neutral cluster and has been extrapolated to establish the metal-nonmetal transition to occur around 400 atoms. This work and more recent higher resolution studies[25] have also yielded vertical binding energies (VBEs) for a wide size range of Hg_n^- clusters.

Dynamical processes in Hg clusters have received less attention. Time-resolved fragmentation and ionization experiments[26] showed evidence for coherent wave packet dynamics at early times, and for the production of multiply charged fragments at laser intensities as low as $10^{11}\,W/cm^2$. Busani *et al.*[15] have measured wavelength-dependent PE spectra of Hg_n^- anions and found evidence for $p \leftarrow s$ excitation, followed by electron-hole recombination and ejection of a photoelectron via Auger decay.

In this paper, we explore electronic relaxation dynamics in size-selected Hg_n^- ($n=11-18$) anions using time-resolved photoelectron imaging (TRPEI), a pump-probe experiment in which one measures the time-evolving photoelectron kinetic energy and angular distribution from electronically excited clusters. The utility of this and related techniques in following nonradiative dynamics in molecules and clusters has been amply demonstrated.[27,28] We focus on *intraband* relaxation dynamics of these clusters. Using a 100 fs pump pulse, we excite the single *p* electron, initially in the lowest molecular orbital of the *p*-band, to an excited state within this band lying below the detachment limit. We then probe the resulting nonstationary state using a delayed probe of similar duration, which detaches the electron, and by imaging of the photoelectrons obtain their kinetic energy and angular distributions as a function of pump-probe delay, enabling us to track the relaxation dynamics of the excited *p* electron.

This experiment offers several noteworthy features. First, since the anion clusters are charged species, they can be (and are) mass-selected prior to spectroscopic investigation, removing any ambiguity as to the size of the cluster. Second, the pump photon energy, 1.5 eV, is less than the *s*-*p* band gap, so the electronic excitation only involves excitation of a single *p* electron and for the same reason, dipole-dipole induced interband excitations cannot be involved in the relaxation dynamics. This situation differs from the electronic spectroscopy of neutral and positively charged mercury clusters which involves a complex mixture of single and collective electronic excitation.[29] Finally, as was demonstrated in our recent studies of C_6^- ,[30,31] TRPEI not only yields lifetimes for the initially excited species but also allows continuous tracking of the relaxation dynamics through multiple electronic states.

The key results in this work are that the intraband relaxation dynamics occur on a time scale of tens of picoseconds, considerably slower than was observed in small transition metal cluster anions.[12,13] There are significant variations in the relaxation rates with cluster size, with Hg_{11}^- showing a particularly long-lived initially excited state. We attribute the observed dynamics to sequential radiationless transitions between close-lying excited electronic states, essentially the cluster analog of electron-phonon coupling; electron-electron scattering effects seen in previous TRPES experiments on metal cluster anions are largely absent here because the *p* band, in which all the dynamics occur, is singly occupied.

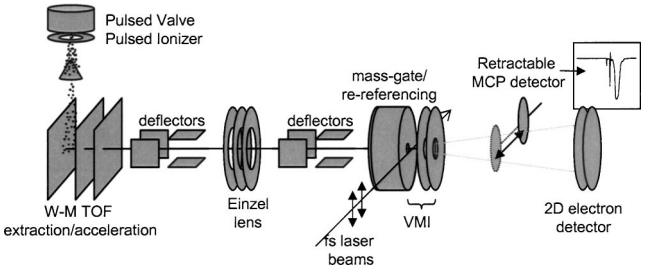

FIG. 1. Schematic of the main components of the TRPEI instrument.

Furthermore, other decay channels such as interband excitation are blocked as the band gap is greater than the photon energy. The observed dynamics reflect pure electron-nuclear relaxation, comparable to electron-phonon relaxation in the bulk.

II. EXPERIMENT

The experiment has been described in detail elsewhere and only an overview and specifics are presented here.[30,32] The main components of the vacuum system are shown in Fig. 1 where the main difference is that we use a pulsed valve designed for the generation of mercury cluster anions. Mercury clusters are produced by coexpanding 40 psi of Ar and the vapor pressure of Hg at 220 °C into vacuum using an Even-Lavie pulsed solenoid valve[33] operating at 40 Hz. The expansion is intersected by a pulsed electron beam forming cluster anions through secondary electron attachment. These are then extracted perpendicularly into a Wiley-MacLaren time-of-flight mass spectrometer and mass-selected using an electrostatic switch 1.2 m downstream.[34] This mass gate is also used as a re-referencing tube and acts as the first plate of the velocity map imaging (VMI) lens.[35] VMI projects each velocity vector of the ejecting photoelectrons onto a specific point on a two-dimensional (2D) plane. On this focal plane, a 70 mm diameter dual multichannel plate coupled to a phosphor screen yields a visual readout of each event, which is captured using a charge-coupled device (CCD) camera. Typically each laser shot produces between 10 and 20 photoelectrons (depending on cluster size) and images are accumulated over 15 000–20 000 laser shots.

Pump and probe pulses are derived from a commercial Ti:Sapphire oscillator and chirped pulse regenerative amplifier (Clark MXR, NJA-5, and CPA1000). The output from the amplifier is recompressed to give 100 fs pulses around 800 nm. In one-color experiments, we use either this laser pulse at a photon energy of 1.57 eV, or frequency-doubled/tripled light at 3.15/4.58 eV. In two-color experiments, the fundamental at 1.53 eV is split into two parts: a pump and probe beam. The probe is frequency-doubled in BBO yielding 90 μJ/pulse around 3.06 eV. The remainder is used for the pump (50 μJ/pulse) and is directed onto a motorized delay stage generating a relative pump-probe delay and subsequently recombined collinearly, prior to focusing in the vacuum chamber. We estimate the intensity in the interaction region to be on the order of $10^{11}\,W/cm^2$. The polarization axes of both pump and probe are parallel to the detector ensuring the 3D photoelectron cloud has cylindrical symme-

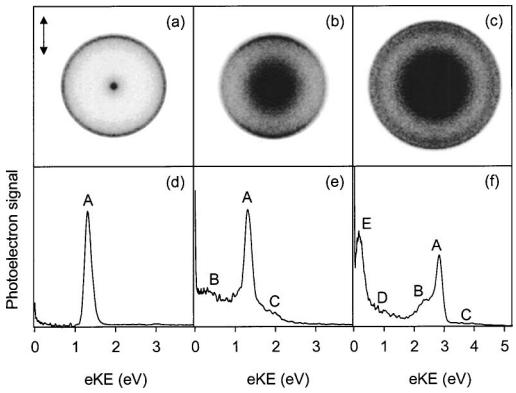

FIG. 2. Symmetrized photoelectron images for (a) Hg_{14}^- detached with 1.57 eV, (b) Hg_{14}^- detached with 3.15 eV, and (c) Hg_{14}^- detached with 4.58 eV. Their corresponding photoelectron spectra are shown in (d)–(f), respectively. The laser polarization direction is indicated by the arrow. Labeling of features corresponds to Fig. 3.

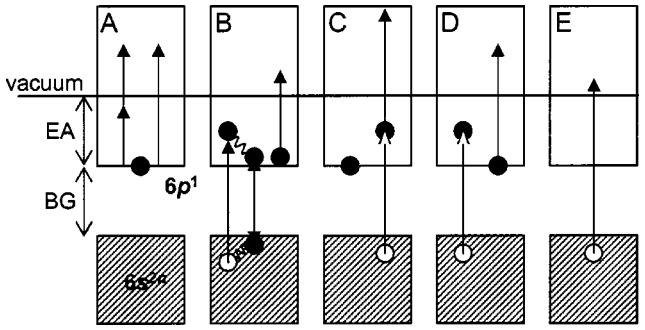

FIG. 3. Diagram describing all labeled processes observed in Fig. 2. The labels here correspond to the features in Fig. 2. neutral. In A, relevant states are assigned and are the same for all other panels. BG is the band gap and EA the electron affinity of the neutral cluster. Upwards arrows indicate excitation, the length of which indicate the photon energy.

try, thus allowing for the reconstruction of this 3D cloud from its measured 2D projection, which we do using a variation of the BASEX (Basis-Set Expansion Abel Transform) routine.[36] PE spectra are generated by angular integration of a slice through the center of the 3D reconstruction and conversion from velocity to energy space. The kinetic energy resolution is typically 5%, some of which is from the ~20–25 meV bandwidth of our pulses. Photoelectron angular distributions (PADs) are immediately available from the data. Generally, the anisotropy of a PAD is defined by an anisotropy parameter β_2 which we obtain by radially integrating the inverted image over the feature of interest.

Finally, we can monitor fragmentation of mass-selected clusters following pump-only irradiation. This is accomplished by detecting ions on a retractable dual multichannel plate (see Fig. 1), which intersects the ion beam path some 30 cm beyond the laser interaction region. Parent and daughter ions emerge with different speeds from the static electric fields of the VMI lens and thus are temporally separated en route to the retractable detector (see inset, Fig. 1) In this manner, the existence and extent of cluster fragmentation is determined. Unfortunately, no temporal information about the fragmentation process is gained.

III. RESULTS AND ANALYSIS

A. One-color PEI

Figures 2(a)–2(c) show symmetrized PE images collected following one-color detachment of Hg_{14}^- at 1.57 eV, 3.15 eV, and 4.58 eV, respectively. Figures 2(d)–2(f) show their corresponding PE spectra. Rings at larger diameter in the images correspond to peaks at higher electron kinetic energy (eKE) in the PE spectra. The vertical binding energy (VBE) and s-p band gap (BG) are 1.87 and 2.2 eV, respectively, for this cluster.[14,25] Several physically distinct mechanisms contribute to the one-color PE spectra. Each feature is labeled to indicate its correspondence with the various photodetachment schemes as shown in Fig. 3.

Excitation at 1.57 eV shows an outer ring in the image (the central spot is discussed below) corresponding to peak A, which is about 200 meV wide, in the PE spectrum. This peak is from two-photon detachment of the single electron occupying the lowest molecular orbital of the p band (see Fig. 3). The photoelectron peak is very intense for a two-photon process and suggests resonance enhancement via excited states within the p band. Excitation with 3.15 eV exceeds the VBE of Hg_{14}^- and so in Fig. 2(e), a single distinct peak is present (labeled A) corresponding to direct detachment of this p electron with a single photon. Both features labeled A in Figs. 2(d) and 2(e) are centered at 1.3 eV, in accord with the VBE of Hg_{14}^-.

Figure 2(e) also shows a broad feature at low kinetic energy (B) and a high-energy shoulder extending to about 2.0 eV (C). These extra features appear because the photon energy, 3.15 eV, is greater than the band gap and can therefore excite electrons from the s to p bands. The high-energy shoulder extending past 2.0 eV shows quadratic laser power dependence. We assign this feature (C) to a resonance enhanced interband two-photon detachment process: excitation of an s electron to a $6s^{2n-1}6p^2$ configuration followed by detachment of the same electron, leaving the neutral in the excited $6s^{2n-1}6p^1$ state. The first step involves excitation from the s band, which is full. All electrons in this band are optically active and those with energies $h\nu$-BG below the top of the s band contribute to the photoelectron feature C. The maximum kinetic energy of the photoelectrons for this process is $\mathrm{eKE}_{\max}=2h\nu-(\mathrm{EA}+\mathrm{BG})\sim 2.2\,\mathrm{eV}$ for Hg_{14}^-, in accord with the observed PE spectrum.

Feature B is attributed to the ejection of Auger electrons following single-photon absorption. The incident photon excites an electron from the full s band to the p band, creating an electron-hole pair. Thermalization of the electrons and hole is in competition with electron-hole recombination, which is accompanied by ejection of the second p electron in a concerted Auger process.[15] This Auger electron contributes to the PE Spectra as a low-energy shoulder relative to direct detachment of the p electron.

Detachment with 4.58 eV photons produces PE spectra similar in appearance to those presented by Busani *et al.*[15] for excitation at similar energies. Briefly, features A, B, and C have the same origin as the features in Fig. 2(e) and are depicted in Fig. 3. Photoelectrons contributing to feature E

arise from direct one-photon detachment from the *s* band, leaving the neutral in the excited $6s^{2n-1}6p^1$ excited state. The VBE for detachment of the *s* electron is about 4.1 eV. The difference between the onset of this broad feature and detachment of the *p* electron to the neutral ground state presents a direct measure of the band gap of the neutral.[14] Feature D shows quadratic power dependence. It may be an extension of feature C, simply involving two-photon detachment deeper into the *s* band, or it may be from process D in Fig. 3: excitation of an *s* electron to a $6s^{2n-1}6p^2$ configuration of the anion, followed by detachment of the electron at the bottom of the *p* band, leaving the neutral in the $6s^{2n-1}6p^{1*}$ excited state.

The PE spectra of Busani *et al.* were collected using a magnetic bottle, which is relatively insensitive to very low-energy electrons. Imaging, on the other hand, does not suffer from this limitation and very low kinetic energy photoelectrons are collected with high efficiency.[37] A peak at zero energy is seen in all three PE spectra. This corresponds to the bright spot in the center of the PE images in Fig. 2(a) and is also present in Figs. 2(b) and 2(c) although, in order to reveal other features in the latter two, saturation at the center has obscured this. These slow electrons probably originate from thermionic emission similar to low-energy electrons observed for C_n^- clusters.[38,39] The time scale of such delayed emission is typically on the order of many nanoseconds[40] and is not expected to compete with any of the processes in Fig. 3 nor with decay dynamics described below.

Finally, TRPEI measures PADs from which we extract anisotropy parameters. The PAD at a given eKE may be expressed as[41]

$$I(\theta,\epsilon)=\frac{\sigma}{4\pi}[1+\beta_2 P_2(\cos\theta)+\beta_4 P_4(\cos\theta)+\cdots],$$

where θ is the angle between the laser polarization and the ejected photoelectrons at energy ϵ, σ is the total cross section, and $P_l(\cos\theta)$ are *l*th-order Legendre polynomials weighted by the anisotropy parameters β_l. For *n*-photon transitions, $l=0,2,...,2n$. Anisotropy parameters provide insight into the detachment process, and thus the nature of the ground anion state. This is particularly so for single photon transitions, where β_4 is omitted. Feature A is perhaps the most informative from this perspective as it involves direct detachment of the ground state anion to the ground state neutral.

Figure 4 shows β_2 values for feature *A*, radially integrated over the full width at half maximum, for a range of clusters detached at 3.15 eV. The β_2 values show rather erratic behavior up to Hg_{15}^-, indicating that the nature of the neutral LUMO is changing quite dramatically over this cluster range. Specifically, Hg_8^- and Hg_9^- show very anisotropic detachment ($\beta_2=1.3$ and 1.4, respectively), whereas Hg_{12}^- shows an almost isotropic distribution ($\beta_2=0.1$). For cluster Hg_{15}^- and larger, the β_2's behave more smoothly and decrease gradually from $\beta_2=0.7$ for Hg_{15}^- to $\beta_2=0.6$ for Hg_{20}^-.

In measuring the values of β_2 for the direct detachment feature, we cannot account for the contributions from overlapping features such as B and C. In particular, feature B is unavoidable at 3.15 eV for clusters whose band gap is less than this energy ($Hg_n, n>12$). Feature C is minimized by ensuring that the intensity is sufficiently low.

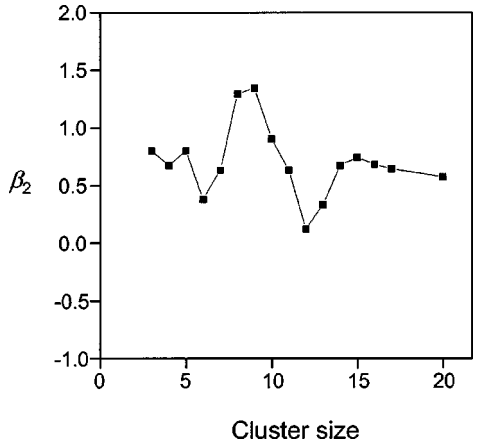

FIG. 4. Anisotropy parameters β_2 for one-photon detachment of the *p*-band electron at 3.15 eV photon energy for clusters Hg_n^- in the size range $3\leqslant n\leqslant 20$.

Finally, we point out that the PAD produced from the Auger electrons (feature *B*) is isotropic, $\beta_2\sim 0.0$, for all the clusters in which this feature was present. This is expected and in accord with the findings of Busani *et al.*[15]

B. Pump-probe dynamics for Hg_n^- ($11\leqslant n\leqslant 16, n=18$)

Figure 2(a) shows photodetachment occurs via intraband excitation of the *p* electron to excited electronic states within the band. This result suggests we can perform two-color pump-probe experiments to follow the dynamics within the *p* band subsequent to intraband excitation, using the scheme shown in the top panel of Fig. 5. Specifically, as the excited electron relaxes, the probe-induced PE spectrum should shift toward lower eKE.

Typical pump-probe PE images and spectra are presented in Figs. 5(a)–5(c) for the Hg_{15}^- cluster for pump-probe delays of 0, 8, and 62 ps, respectively. Near $t=0$, the PE image shows two major features: an intense, anisotropic ring and a fainter ring at larger diameter. Spectra at later times show the outer ring becoming more diffuse and shrinking in diameter, while the inner ring is unchanged. The corresponding PE spectra show that the inner ring transforms to a sharp peak at eKE=1.15 eV. This feature is from mechanism A seen in the one-color spectra and is labeled as such: a combination of one-photon detachment of the *p* electron of the probe and two photon detachment by the pump with VBE =1.91 eV for Hg_{15}^-. Processes B and C [Fig. 2(e)] also contribute. However, the main feature of interest is the outer ring, since this is clearly dependent on the pump-probe delay. At $t=0$, it transforms to a relatively narrow feature at eKE =2.7 eV. At 8 ps [Fig. 5(b)], the two-color signal has shifted toward lower eKE and broadened considerably. By 62 ps [Fig. 5(c)], it appears as a shoulder on the high-eKE side of peak A.

A more detailed view of the time-evolving spectra is given in Fig. 6, where we show time-dependent PE spectra progressions at pump-probe delay increments of 6.7 ps for Hg_{11}^- (a) and 3.3 ps for Hg_{15}^- (b). In order to emphasize the

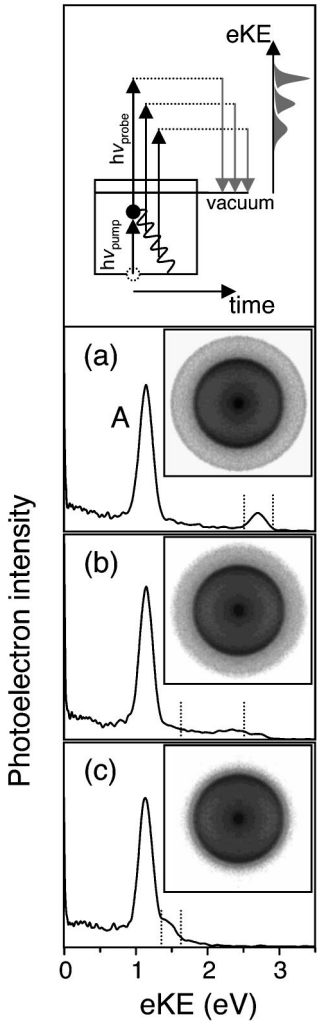

FIG. 5. Time-resolved photoelectron spectra for Hg_{15}^- excited with 1.53 eV and probed by 3.06 eV at time $t=0$ ps, $t=8$ ps, and $t=62$ ps in (a)–(c), respectively. The insets show the symmetrized time-resolved photoelectron images from which the spectra were extracted. Vertical dashed lines indicate energy windows representative of the main dynamical features. The upper panel shows a schematic diagram of the excitation scheme and dynamics in the *p*-band.

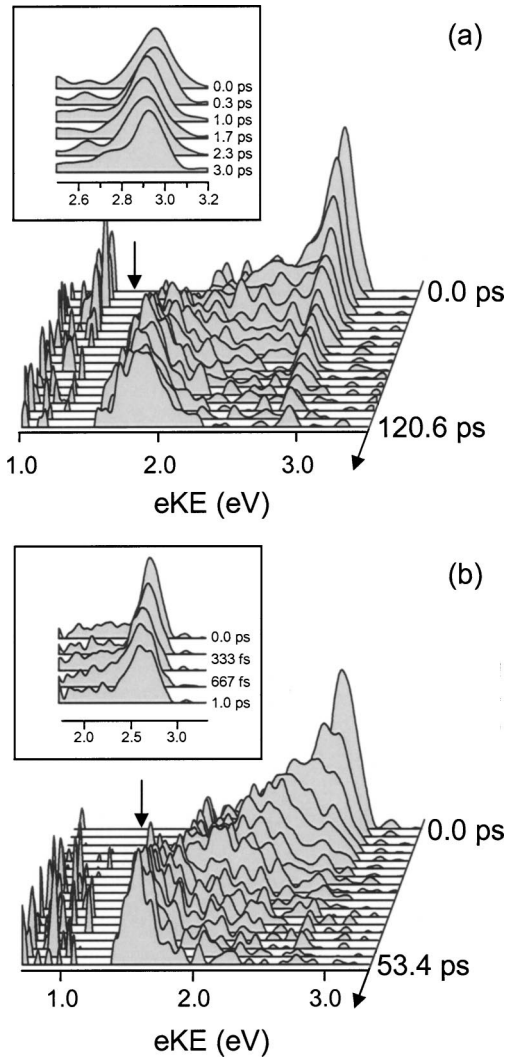

FIG. 6. Time-resolved photoelectron progression for (a) Hg_{11}^- and (b) Hg_{15}^- excited at 1.53 eV and probed 3.06 eV. A $t<0$ photoelectron spectrum has been subtracted to remove the two-photon features (C in Fig. 2) and to reveal only the two-color time-dependent photoelectron signal. The eKE corresponding to direct detachment from the ground state is depicted by vertical arrows. The time step between spectra in (a) is 6.7 ps and in (b) is 3.3 ps. The insets show the temporal dynamics at very early times.

two-color signal, a probe-before-pump spectrum is subtracted from all the plots. This procedure results in negative signal in the region of peak A (vertical arrow), since the depletion of peak A induced by the pump pulse is absent in the probe-before-pump spectrum. For clarity, all negative intensities are set to zero in Fig. 6.

At $t=0$ ps, the excited *p* electron produces a photoelectron peak which is very similar in shape and width, about 200 meV at FWHM, to that produced by direct detachment of the electron from the bottom of the *p* band. For Hg_{15}^-, the signal then gradually shifts towards lower kinetic (higher binding) energy and spreads. At long times, $t>50$ ps, the PES has evolved into a peak centered at eKE=1.5 eV, that is, only slightly broader than the $t=0$ peak, and no further dynamics occur. This long-time signal does not merge completely with that of the unexcited cluster but instead extends to higher eKE. The general pattern of spectral evolution in Fig. 6(b) is seen for every cluster studied here except Hg_{11}^-, shown in Fig. 6(a). For this cluster, the initially prepared state persists for significantly longer. At times in excess of 100 ps, there still remains a well-defined photoelectron peak, which has not spread but has simply dropped in intensity. At the same time, some of the signal does shift to lower eKE and reforms a peak at long times, just as in the larger clusters.

We point out that Hg_{11}^- was the smallest cluster studied here and has the lowest VBE=1.73 eV, just above the pump photon energy. For smaller clusters, $h\nu_{\text{pump}}>\text{VBE}$ and the PE spectra are dominated by one-photon direct detachment, for which the cross section is apparently so large that any resonant two-color signal is depleted beyond the point where it can be observed. Dynamics in these smaller clusters are discussed in a following publication in which a lower pump photon energy was used.[42]

C. Relaxation rates

The time evolution in the PE spectra represents relaxation of the initially excited *p* electron; as this electron loses

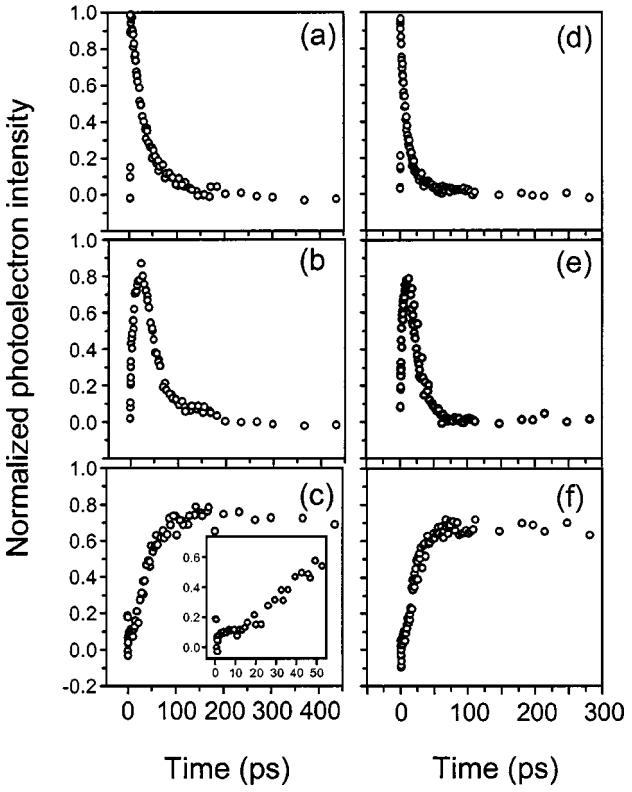

FIG. 7. Normalized integrated photoelectron intensity for spectral windows representative of the main dynamical features. (a)–(c) and (d)–(f) represent the population for the initially prepared stare, the intermediate regime and the final state for Hg_{11}^- and Hg_{15}^-, respectively.

electronic energy, its binding energy increases and its eKE drops. These dynamics can be clocked by measuring the integrated photoelectron intensity in spectral windows of the time-dependent PE spectr. The windows are chosen such that the main dynamical features are monitored, as illustrated in Fig. 5 by the vertical dashed lines. For Hg_{15}^-, the time scale for the decay of the initially prepared excited state is tracked by background subtraction of a probe-pump PE spectrum (see Fig. 5) and integration over the spectral window shown in Fig. 5(a), while dynamics at intermediate and long times are monitored by integrating signal in the windows shown in Figs. 5(a) and 5(b), respectively. Values for the energy windows are cluster-specific as the electron affinity of the clusters increases with size; those in Fig. 5 serve as an example for a typical cluster.

In Figs. 7(a)–7(c) and 7(d)–7(f), we show the results of such an analysis for Hg_{11}^- and Hg_{15}^-, respectively, using the photoelectron data in Figs. 6(a) and 6(b). Integrated intensities in the high-, intermediate, and low-eKE windows are shown in (a) and (d), (b) and (e), and (c) and (f), respectively; normalization is with respect to the maximum signal in the high-eKE window (top panels). For all clusters, the drop in intensity of the initially prepared state is well fit with an exponential decay with size-dependent time constants given in Table I. As the initially prepared state decays, population migrates into the intermediate window, which grows accordingly and then decays. The signal in the low-energy window, monitoring the long-time dynamics, remains constant at early times [see inset in bottom panel of Fig. 7(c)], as

TABLE I. Lifetimes for initially excited states in Hg_n^- clusters.

Size	Relaxation time (ps)	Error
11	33.9	±0.7
12	13.5	±0.3
13	6.6	±0.3
14	13.8	±0.9
15	10.3	±0.2
16	7.5	±0.6
18	8.0	±0.4

it takes several picoseconds for the population to reach this spectral window. This signal then rises and flattens over a period of several tens of picoseconds after which no more dynamics are observed.

The asymptotic signal levels in Figs. 7(c) and 7(f) are only 0.7–0.8, reflecting the observation that the integrated signal level in the long-time window is less than that in the short-time window. The apparent loss of total population at long times reflects the fact that some of this signal occurs in a region of overall negative intensity resulting from our background subtraction procedure. This effect can be seen more clearly in Fig. 5(c), which is not background-subtracted, showing the shoulder at long times merging with the one-color peak A. Fitting two Gaussian profiles to this long-time PE spectrum does indeed reveal that about 30% is lost to the main feature; the two peaks are separated by 0.28 eV. In any case, the observation that most the signal at long times is shifted to higher eKE from peak A is significant and discussed in Sec. IV.

As a further means of characterizing the dynamical evolution of the excited electron with time, we have considered the average eKE for the photoelectron feature due to this electron by calculating the first moment of the photoelectron signal with respect to the energy. This is plotted on Fig. 8 for cluster Hg_{15}^-. The most striking feature of this plot is the apparent linearity from 2 ps to about 50 ps and has been observed for all clusters. The average kinetic energy then evolves towards its final value, indicating the end of the observed dynamics.

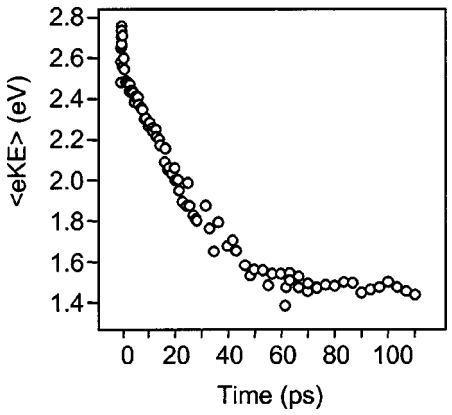

FIG. 8. Average electron-kinetic energy ⟨eKE⟩ of the two-color time-dependent signal for Hg_{15}^-.

D. Fragmentation

Using the scheme indicated in Fig. 1, we have monitored fragmentation of the mass-selected clusters following interaction with a pump-only beam (1.5 eV). Generally, hot clusters may dispose of excess energy by evaporation if the cluster is bound by weak forces or thermionic emission, when the electron affinity is much less than the energy required to break internal bonding. We may expect evaporation as the mercury clusters considered in this size range are relatively weakly bound due to the van der Waals nature present in the bonding.

For all mass-selected clusters studied, Hg_n^- ($n=11-15,18$), we have observed anionic daughter ions. A typical example of a mass spectrum is shown in the inset of Fig. 1 for Hg_{11}^-, indicating the arrival of two daughter ions prior to the parent ion. For Hg_n^- ($n=11-13$) we see both Hg_{n-1}^- and Hg_{n-2}^- daughter ions, where the relative intensity of Hg_{n-2}^- increases from the weaker peak to the overwhelmingly dominant peak. In the range $n=14-15$, we observe Hg_{n-1}^-, Hg_{n-2}^-, and Hg_{n-3}^- daughter ions although for Hg_{14}^-, the Hg_{n-1}^- peak is very small. Finally, for Hg_{18}^-, we again only observe the loss of up to two atoms to leave Hg_{17}^- and Hg_{16}^-. We stress that the evaporation studies are more designed toward demonstrating the existence of fragmentation as opposed to extracting accurate photofragment branching ratios. In particular, it is possible that the true Hg_{n-1}^- daughter ion and even the Hg_{n-2}^- daughter are obscured by the rather broad parent peak. Hence, the fragmentation patterns given here represent ''lower bounds'' on the extent of dissociation; the daughter ions may actually be smaller by one or two Hg atoms.

IV. DISCUSSION

In this section, we first consider qualitative aspects of the TRPE spectra and the electronic structure of the mercury clusters studied here. The shifting of the two-color photoelectron peak towards lower eKE is interpreted in terms of electronic relaxation of the initially prepared state, with the excited electron ultimately ending up at or near the bottom of the p band from whence it came. We then propose a simple kinetic model based on sequential radiationless transitions among the electronic states of the p band that reproduces the main features of our results. This electronic relaxation is accompanied by vibrational excitation of the cluster, resulting in vibrationally hot clusters at the longest delay times probed in the experiment. At very short delay times, rapid shifts of the eKE are attributed to wave packet motion on the initially excited multidimensional potential energy surface. At the longest delays, we take into account the effects of the vibrational heating on the PES and consider the possibility of ultrafast evaporation. Cluster size effects are discussed in terms of the observed relaxation rates for the range of clusters studied. In particular Hg_{11}^- relaxes significantly slower than the other clusters.

A. Overall relaxation dynamics

TRPES allows one to track excited state anion dynamics by correlating the eKE following probe detachment to the energetics of the system under investigation. The photoelectron eKE may be expressed as

$$\mathrm{eKE}=h\upsilon_{\mathrm{probe}}-\mathrm{EA}+E_{\mathrm{anion}}-E_{\mathrm{neutral}}, \tag{1}$$

where EA is the size-dependent electron affinity of cluster Hg_n, E_{anion} is the total internal (electronic+vibrational) energy of the cluster following pump excitation, and E_{neutral} corresponds to the internal energy of the neutral formed by photodetachment. Note that the neutral clusters are formed in their ground electronic state; the first excited state, corresponding to a $6s^{2n-1}6p^1$ configuration, is not energetically accessible by one-photon detachment at 3.06 eV.

In the absence of fragmentation or photon emission, E_{anion} is constant with time. However, energy partitioning between electronic and vibrational degrees of freedom will evolve following pump-induced electronic excitation within the p band. The photoelectron spectrum at a given pump-probe delay time then represents a Franck-Condon mapping of the anion vibronic wave function $\Psi_{ev}^{(-)}(t)$ onto the ground electronic state of the neutral cluster.[28] More specifically, one expects that electronic energy is converted into vibrational energy over time. Thus, while electronic relaxation tends to shift the photoelectron eKE toward lower values, the accompanying vibrational heating partially compensates for this via vibrational hot band transitions. This latter effect depends on the geometry change between the various anion electronic states and the neutral ground state. If the geometry changes are small, then vibrational heating has minimal effect on the PE spectra because the cluster vibrational modes are largely inactive; as a result, their time evolution can be interpreted rather straightforwardly in terms of electronic relaxation.

There is considerable evidence that this scenario is indeed the case for Hg clusters. PE spectra from direct, p-band detachment are only 200 meV wide [Fig. 2(e), for example], indicating small geometry changes between the anion and neutral ground state. The pump-probe spectra at $t\cong 0$ are similarly narrow, showing that the geometries of the initially excited state and neutral ground state are similar. Finally, although the TRPE spectra exhibit considerable spreading at intermediate times, a relatively narrow peak is seen at the longest times, when the vibrational energy should be maximal. Hence, the overall observed dynamics reflect primarily the time-dependent *electronic* energy of the excited cluster.

There are many instances in the literature[28] in which TRPES has been used to follow the dynamics of radiationless transition in molecules. In such experiments the manifold of electronic states is relatively sparse; as a result, features in the PE spectra are readily assigned to individual electronic states, from which state-specific lifetimes may be extracted. In contrast, for the mercury clusters studied here, the density of electronic states participating in the dynamics is much higher, and the evolution of the time-dependent PE spectra suggests bulklike continuous relaxation for the excited electron back to its ground state. However, the assumption of a continuum of electronic states is an oversimplification. There are $3n$ electronic states for cluster Hg_n in the p

band. The width of the band is cluster-dependent[23] and ranges between about 4.0 eV for Hg_{11} and 4.6 eV for Hg_{18}, implying an average density of states (DOS) ranging between 8 states/eV and 12 states/eV, respectively. The observed initial state lifetimes (Table I) imply homogeneous linewidths (<1 meV) that are much smaller than the spacing between electronic states (~100 meV), so in the size range under consideration, the *p* band is best considered as a dense but discrete set of electronic states.

B. Kinetic modeling of TRPE spectra

In this section, we put forth a simple kinetic model for the TRPE spectra based on the ideas enumerated above. For simplicity, we consider the electronic states within the *p* band to be distributed evenly, reflecting an *average* electronic DOS as mentioned before. Electronic excitation introduces 1.5 eV of energy into the system, which defines the initial conditions. We may then calculate the evolution of the electronic energy with time using kinetic rate equations of the form

$$\frac{dN_i}{dt} = \sum_{j<i} k_{ji} N_j - \sum_{j>i} k_{ij} N_i , \tag{2}$$

where we have labeled the states involved as $i=1,2,3,...$ in descending energy order. N_i and N_j represent the population probability in state *i* and *j*, respectively, and these states are coupled together through rate constants k_{ij}. The first term accounts for population contributing to state *i* from higher lying electronic states, *j*; the second term allows for population to be removed from state *i*, which is transferred to lower-lying electronic states, *j*. The rate constants, k_{ij}, depend on the energy gap between state *i* and *j*, such that

$$k_{ij} = k e^{-\Delta E_{ij}}, \tag{3}$$

where *k* is a rate constant and ΔE_{ij} is a scaled energy gap, given by $(j-i)\Delta E_{av}^{(n)}/0.110$, where $\Delta E_{av}^{(n)}$ is the average spacing between adjacent energy levels for Hg_n, and 0.110 eV is the average energy spacing for all the clusters studied here. $\Delta E_{av}^{(n)}$ and the overall average of 0.110 eV are estimated from the calculations by Pastor and Benneman,[23] which show that the *p*-band width scales approximately as $n^{1/3}$, so that $\Delta E_{av}^{(n)} \propto n^{-2/3}$. Initial conditions at $t=0$ are $N_1 = 1$, and $N_{i>1} = 0$, where state 1 lies 1.5 eV above the bottom of the band.

In Fig. 9(a), we show the time-dependent populations of Hg_{15}^- for excitation at 1.5 eV, an average DOS of 10 states/eV, and where we have chosen $k_{i,i+1}$, the radiationless transition rate between adjacent levels, to be 0.1 ps^{-1}. The origin of the spreading is immediately recognizable in Fig. 9(a): population rapidly migrates into a number of excited states before being totally relaxed. As a number of states at a given time during the decay process have appreciable population, the electron has effectively spread over a range of energy levels.

We may convert the time-dependent populations to a PE spectrum progression, as a direct comparison with our experiment, by simply convoluting the time-dependent populations with a Gaussian with a full width at half maximum of

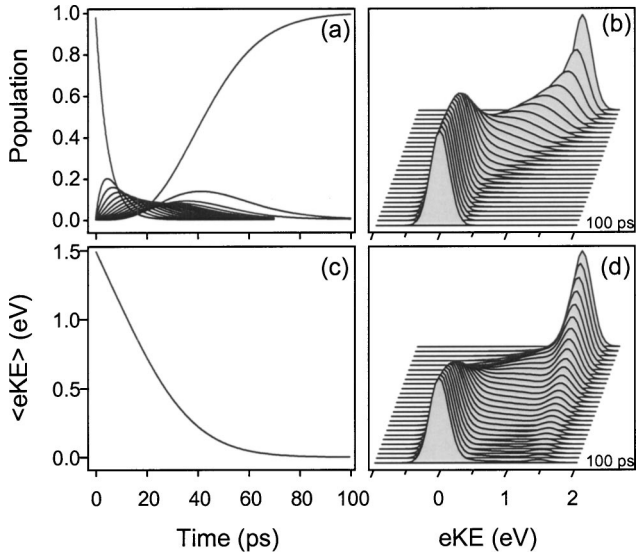

FIG. 9. Numerical results from a kinetic model (see text). (a) Normalized time-resolved population for the *p*-band states included in the calculation, illustrating population shift from initially excited state at short times to ground state by 100 ps. (b) Corresponding time-resolved photoelectron spectra, which should be compared Hg_{15}^- results in Fig. 6(b). (c) Time-dependent ⟨eKE⟩ for the PE spectra in (b). (d) TRPEI spectra calculated with kinetic model in which initial relaxation rate is lowered by factor of 6. Compare to Hg_{11}^- results in Fig. 6(a).

200 meV. This width was set to reflect the direct detachment observed experimentally. The PES progression is shown in Fig. 9(b) and shows remarkable qualitative agreement with Fig. 6(b) considering the simplicity of the model. At early time, a well-defined peak is observed, which rapidly spreads and shifts to lower eKE. Relaxation is complete by 60 ps, by which time only the lowest electronic level of the *p* band is populated. The dynamics may be further characterized by considering the average eKE with time of the excited electron, directly comparable to Fig. 8, where the average eKE is shown for the relaxation in Hg_{15}^-. This has been shown in Fig. 9(c), where again, the model reproduces the most prominent feature of the experimentally observed average eKE—the linearity as the electron cascades towards the bottom of the band.

The question arises as to whether this model can be modified to reproduce the anomalous results found for Hg_{11}^- in which the initially excited state appears to persist for a much longer time than for the larger clusters studied here. In fact, we found that by reducing k_{ij}, where $i=1$, by a factor of 6 relative to the other rate constants yielded the calculated PE spectrum progression shown in Fig. 9(d). Comparing this result with the experimentally observed TRPEI spectra for Hg_{11}^- in Fig. 6(a) reveals excellent overall qualitative agreement. The initially excited state acts as a bottleneck and once population leaves this excited state, it reaches the initial ground state quickly.

There are, however, two aspects of the experimental spectra not reproduced by our kinetic model. These are considered in the following sections.

C. Dynamics at early delays

There is considerably more evolution of the PE spectra during the first 1–2 ps than predicted by the model. The insets in Fig. 6 emphasize the early-time dynamics seen for Hg_{11}^- and Hg_{15}^-. For Hg_{15}^-, the average eKE drops by about 150 meV in the first picosecond. For Hg_{11}^-, the peak also drops to lower eKE, by about 100 meV, but then returns by about 3 ps. We attribute both observations to nuclear wave packet dynamics in the initially excited anion state resulting from coherent excitation of closely spaced vibrational levels. This requires some Franck-Condon activity in the excitation process, presumably from relatively small displacements in the equilibrium geometries of the ground and initially excited states of the cluster anions. The apparent recurrence at early times in the Hg_{11}^- spectrum is a particularly unambiguous signature of such dynamics. The longer lifetime of the initially excited state in Hg_{11}^- allows more time for the wave packet dynamics to evolve prior to electronic relaxation, and once this process begins the subsequent dynamics are modeled by Eq. (2). Although we see these effects, they are not prominent enough to extract information about the upper state vibrational dynamics. These are more clearly observed for smaller clusters and will be discussed in detail elsewhere.[42]

D. PE Spectra at long delays

Once the PE spectra have stopped evolving, the experimental spectra show significant signal at higher eKE than feature A from the anion ground state, as can be seen in Fig. 6 by comparing the displacement of the peak at the longest pump-probe time to the vertical arrow. This shift, not seen in our kinetic model, ranges from ~400 meV for Hg_{11}^- to 100 meV for Hg_{18}^-. As pointed out in Sec. III C, this shifted signal represents about 70%–80% of the signal seen at the earliest delay times (also see Fig. 7), so it cannot simply be ignored as a small ''tail'' remaining from our background subtraction procedure.

The shifted signal is attributed to thermal effects—excitation of the internal vibrational modes of the cluster—as electronic relaxation proceeds. However, internal excitation may have differing consequences. At long times, we may be photodetaching ''hot'' anion ground state, where the cluster has the 1.5 eV of excess energy distributed amongst its $3n-6$ internal modes. Alternatively dissociation may occur on a time scale comparable to relaxation and we may be detaching ground state anion from a cluster smaller than the parent ion. In the former scenario, detachment from a vibrationally hot anion leads to significant spectral broadening of the PE spectrum owing to hot band transitions, while evaporation results in smaller anions with lower VBEs. Both effects yield faster electrons than would be seen from the vibrational ground state of the parent ion.

We consider both effects in more detail to assess which may be dominant. Once electronic relaxation is complete, 1.5 eV of excess energy may be stored in the $3n-6$ vibrational modes, corresponding to about 55 meV/mode and 31 meV/mode for Hg_{11}^- and Hg_{18}^-, respectively. These energies are considerably less than the shifts in the long-time PE spectra. Given that we have argued that there are only small changes in equilibrium geometry, resulting in small Franck-Condon factors for off-diagonal (i.e., hot band) transitions, it would seem that vibrational heating cannot explain the long-time shifts. However, mercury clusters are weakly bound clusters with very low frequencies; calculations by Flad *et al.*[43] yield an average frequency of 34 cm^{-1} (4.2 meV) for Hg_6, for example. Hence, each mode has significant vibrational excitation, and the resulting large amplitude motion is quite likely to render inadequate the standard Franck-Condon picture of photoelectron spectroscopy based on separable harmonic oscillators.

The shifted PE spectra at long times may also be a signature of evaporation, because the VBEs of Hg_n^- clusters generally drop as the cluster becomes smaller.[14] Excitation at 1.5 eV is certainly sufficient for evaporation of multiple Hg atoms. We observe fragmentation using the scheme illustrated in Fig. 1. Moreover, the average cohesive binding energy per atom in the anion clusters, $E_{\mathrm{coh}}^{(-)}(n)$, can be estimated from the relation

$$E_{\mathrm{coh}}^{(-)}(n)=E_{\mathrm{coh}}^{(0)}(n)+\mathrm{VBE}/n, \tag{4}$$

where $E_{\mathrm{coh}}^{(0)}(n)$, the corresponding value for neutral Hg clusters, has been measured[20] and calculated.[22] Equation (4) yields $E_{\mathrm{coh}}^{(-)}(n)=0.25\,\mathrm{eV}$ for Hg_{13}^-, for example. The question here is one of kinetics. In other words, does at least some evaporation happen on the ~100 ps time scale probed in these experiments, and can such a process be distinguished from vibrational heating?

There is in fact evidence for evaporation on this timescale based on the trends in long-time shifts vs cluster size. A plot of VBE vs n for Hg_n^- clusters[14] shows a significant decrease in slope starting around $n=10$. As a result, for example, the loss of three Hg atoms from Hg_{11}^- results in a decrease in the VBE by 0.36 eV, while evaporation of three atoms from Hg_{15}^- drops the VBE by only 0.12 eV.[25] These energetic trends are in accord with the experimental size-dependent shifts, and the degree of evaporation required to produce these shifts is to some degree consistent with the fragmentation results discussed in Sec. III D. Thus, while vibrational heating accompanying electronic relaxation can be responsible for some of the shift in the long-time PE spectra, there is reasonably strong evidence that evaporation of two to three atoms occurs on the time scale of the pump-probe experiment; this evaporation is reflected as a perturbation on the electronic relaxation dynamics that dominate the time-dependent PE spectra.

E. Size-dependent relaxation rates

The relaxation rates (ps^{-1}) for of the initially prepared excited state in the p band obtained from the time scales in Table I are shown in Fig. 10. The solid line shows how the rate constants would scale if they depended only on the cluster DOS. Here we have fixed k in Eq. (3) so that initial decay rate $k_{i,i+1}$ matches the experimental decay rate for Hg_{15}^-. This value of k is then used for all clusters, with the initial decay rates determined by the average energy gap between

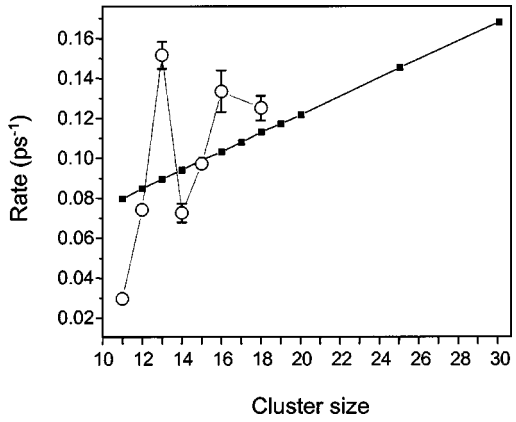

FIG. 10. Relaxation rates for decay of initially excited state for Hg_n^- in the size range $11 \leqslant n \leqslant 18$. Open circles correspond to the experimentally observed time scales and solid squares and solid line indicate the rates determined from kinetic model, where representative electronic DOS were used (see text).

adjacent states according to Eq. (3). These rates increase monotonically with n and provide a useful baseline for comparison with the experimental rates.

The experimental data in Fig. 10 show an overall increase in rate with n but oscillate significantly above and below the solid line, possibly with decreasing amplitude as n increases. This result indicates that the vibronic coupling responsible for the decay of the initially excited state is quite sensitive to the number of atoms in the cluster. In other words, the size regime studied here is such that addition of each atom markedly changes the cluster properties. This conclusion is supported by the size-dependent anisotropy parameters β_2 for detachment from the ground anion state shown in Fig. 4. These exhibit substantial variation with n, indicating that the character of the molecular orbital from which detachment occurs is quite sensitive to the cluster size. Again, we may expect a smoother trend for larger clusters, as here the extra atom will impose a lesser perturbation on the cluster. Interestingly, the cluster revealing the most rapid relaxation is the anion of Hg_{13}, which, if considered purely van der Waals bonded, closes the first highly symmetric icosahedral shell at this size.[44]

Hg_{11}^- shows a significantly reduced rate relative to the other clusters studied. As discussed above, the overall trend in the TRPE spectra indicates that decay of the initially excited state is anomalously slow, and that this cluster is the only one for which the initially prepared state acts as a dynamical bottleneck. The reason for the reduced relaxation rate of this state can only be speculated. There are no clear geometrical or electronic shell motifs present for this particular cluster. We do not, however, rule out the possibility of a polarization-supported state near threshold.[45–47] For Hg_{11}^-, excitation at 1.53 eV promotes the electron to right below the detachment limit at 1.73 eV. Note that this value corresponds to the central peak position in the photoelectron spectra and has a width of ~200 meV at half maximum. We may be accidentally exciting an image-charge bound state, or a state stabilized by induced dipoles within the cluster. The polarizability of Hg clusters is very large due to the very large atomic polarizability of atomic Hg (5.7 Å^3 compared to 4.0 Å^3 for Xe) and collectively due to the van der Waals contributions to the bonding. Polarization-bound states are diffuse states and will consequently have a poor overlap with the molecular orbitals of the cluster causing a dramatic reduction in the rate. Such polarization bound states have, however, not been observed in Hg_n^- but experiments to do so are underway.[48]

Finally, we contrast our observations with similar experiments in metallic clusters. Pontius *et al.*[8–12] performed a series of anion TRPE spectroscopy experiments on small transition metal clusters. Two distinct time scales are seen for Ni_3^- and Pd_n^- ($n=4,7$): a ultrafast sub-100 fs decay due to electron-electron scattering and, once the electron bath has thermalized, a second somewhat slower electron-nuclear relaxation occuring on a 1 ps time scale for Pd_n^- clusters. We see no evidence for electron-electron scattering in our experiment, a reasonable result since we are dealing with a singly occupied electronic band. The electron-nuclear coupling in the Hg_n^- clusters is slower than in the transition metal clusters, most likely because of the high density of electronic states in the latter owing to the open-shell d atoms. The time scales seen in our experiments are intermediate between those seen in TRPE studies of Al_{6-15}^- (200–500 fs),[49] and Au_6^- (~1 ns),[50] two families of clusters with closed d-shell atoms. While these general trends can be rationalized in terms of electronic state densities, a quantitative understanding of these orders-of-magnitude variations in excited state lifetimes is clearly lacking. We hope this growing body of results stimulates a serious theoretical effort to gain more fundamental insights into the factors governing excited state dynamics of these clusters.

V. SUMMARY

Time-resolved photoelectron imaging was used to investigate the dynamics of Hg_n^- ($n=11-18$) cluster anions following intraband excitation at 1.5 eV of the lone electron occupying the p band. These experiments yield the lifetime of the initially excited state and allow one to track the subsequent relaxation dynamics in considerable detail. The excited state lifetimes vary from 6.6 to 33.9 ps, with the $n=11$ lifetime being considerably longer than that of any of the other clusters. The p band in these anions is a dense but discrete manifold of electronic states, and the time-evolving PE spectra can be modeled as a series of radiationless transitions between nearby states, leading to an electronically relaxed but vibrationally hot cluster. The PE spectra at long times show evidence for evaporation of a small number of Hg atoms occurring on a time scale of ~100 ps. The relaxation dynamics and photoelectron angular distributions show a strong dependence on cluster size, indicating that we are still in a size regime where the addition of each atom significantly affects the properties of the cluster. The size range under study here corresponds to the transition between van der Waals and covalent bonding in Hg clusters, and it will clearly be of interest to determine how moving further into the covalent regime will affects trends in the dynamics of these clusters. Dynamical studies following *interband* (i.e.

$s \rightarrow p$) excitation at higher pump energies will also be of interest. These extensions of the work presented here will be carried out in the near future.

ACKNOWLEDGMENTS

This research was supported by the National Science Foundation under Grant No. DMR-0139064. Additional support from the US-Israel Binational Science Foundation is gratefully acknowledged.

[1] A. H. Zewail, Angew. Chem. **39**, 2587 (2000).
[2] M. Cho, PhysChemComm **5**, 40 (2002).
[3] *Clusters of Atoms and Molecules. Theory, Experiment and Clusters of Atoms*, edited by H. Haberland (Springer, Berlin, 1994), Vol. 52.
[4] W. A. de Heer, Rev. Mod. Phys. **65**, 611 (1993).
[5] T. E. Dermota, Q. Zhong, and A. W. Castleman, Chem. Rev. (Washington, D.C.) **104**, 1861 (2004).
[6] W. A. de Heer, K. Selby, V. Kresin, J. Masui, M. Vollmer, A. Chatelain, and W. D. Knight, Phys. Rev. Lett. **59**, 1805 (1987).
[7] W. Hongbin, S. R. Desai, and L. Wang, Phys. Rev. Lett. **77**, 2436 (1996).
[8] N. Pontius, P. S. Bechthold, M. Neeb, and W. Eberhardt, J. Electron Spectrosc. Relat. Phenom. **106**, 107 (2000).
[9] N. Pontius, M. Neeb, and W. Eberhardt, Phys. Rev. B **67**, 035425 (2003).
[10] N. Pontius, G. Lüttgens, P. S. Bechthold, M. Neeb, and W. Eberhardt, J. Chem. Phys. **115**, 10479 (2001).
[11] N. Pontius, P. S. Bechthold, M. Neeb, and W. Eberhardt, Appl. Phys. B: Lasers Opt. **71**, 351 (2000).
[12] N. Pontius, P. S. Bechthold, M. Neeb, and W. Eberhardt, Phys. Rev. Lett. **84**, 1132 (2000).
[13] P. Gerhardt, M. Niemietz, Y. D. Kim, and G. Ganteför, Chem. Phys. Lett. **382**, 454 (2003).
[14] R. Busani, M. Folkers, and O. Cheshnovsky, Phys. Rev. Lett. **81**, 3836 (1998).
[15] R. Busani, T. Giniger, T. Hippler, and O. Cheshnovsky, Phys. Rev. Lett. **90**, 083401 (2003).
[16] J. Koperski, Phys. Rep. **369**, 177 (2002).
[17] C. Bréchignac, M. Broyer, P. Cahuzac, G. Delacretaz, P. Labastie, and L. Wöste, Chem. Phys. Lett. **120**, 559 (1985).
[18] K. Rademann, B. Kaiser, U. Even, and F. Hensel, Phys. Rev. Lett. **59**, 2319 (1987).
[19] C. Bréchignac, M. Broyer, P. Cahuzac, G. Delacretaz, P. Labastie, J. P. Wolf, and L. Wöste, Phys. Rev. Lett. **60**, 275 (1988).
[20] H. Haberland, H. Kornmeier, H. Langosch, M. Oschwald, and G. Tanner, J. Chem. Soc., Faraday Trans. **86**, 2473 (1990).
[21] H. Haberland, B. Vonissendorff, Y. F. Ji, and T. Kolar, Phys. Rev. Lett. **69**, 3212 (1992).
[22] M. E. Garcia, G. M. Pastor, and K. H. Bennemann, Phys. Rev. Lett. **67**, 1142 (1991).
[23] G. M. Pastor and K. H. Bennemann, in *Clusters of Atoms and Molecules*, edited by H. Haberland (Springer, Berlin, 1994), pp. 86–113.
[24] B. Kaiser and K. Rademann, Phys. Rev. Lett. **69**, 3204 (1992).
[25] O. Cheshnovsky (private communication).
[26] B. Bescós, B. Lang, J. Weiner, V. Weiss, E. Wiedenmann, and G. Gerber, Eur. Phys. J. D **9**, 399 (1999).
[27] D. M. Neumark, Annu. Rev. Phys. Chem. **52**, 255 (2001).
[28] A. Stolow, A. E. Bragg, and D. M. Neumark, Chem. Rev. (Washington, D.C.) **104**, 1719 (2004).
[29] S. Grabowski, M. E. Garcia, and K. H. Bennemann, Phys. Rev. Lett. **72**, 3969 (1994).
[30] A. E. Bragg, J. R. R. Verlet, A. Kammrath, and D. M. Neumark, J. Chem. Phys. **121**, 3515 (2004).
[31] C. Frischkorn, A. E. Bragg, A. V. Davis, R. Wester, and D. M. Neumark, J. Chem. Phys. **115**, 11185 (2001).
[32] A. V. Davis, R. Wester, A. E. Bragg, and D. M. Neumark, J. Chem. Phys. **118**, 999 (2003).
[33] U. Even, J. Jortner, D. Noy, N. Lavie, and C. Cossart-Magos, J. Chem. Phys. **112**, 8068 (2000).
[34] W. C. Wiley and I. H. McLaren, Rev. Sci. Instrum. **26**, 1150 (1955).
[35] A. T. J. B. Eppink and D. H. Parker, Rev. Sci. Instrum. **68**, 3477 (1997).
[36] V. Dribinski, A. Ossadtchi, V. A. Mandelshtam, and H. Reisler, Rev. Sci. Instrum. **73**, 2634 (2002).
[37] A. Osterwalder, M. Nee, J. Zhou, and D. M. Neumark, J. Chem. Phys. **121**, 6317 (2004).
[38] B. Baguenard, J. C. Pinaré, F. Lépine, C. Bordas, and M. Broyer, Chem. Phys. Lett. **352**, 147 (2002).
[39] A. E. Bragg, J. R. R. Verlet, A. Kammrath, and D. M. Neumark, J. Chem. Phys. **121**, 3515 (2004).
[40] B. Baguenard, J. B. Wills, F. Pagliarulo, F. Lepine, B. Climen, M. Barbaire, C. Clavier, M. A. Lebeault, and C. Bordas, Rev. Sci. Instrum. **75**, 324 (2004).
[41] K. L. Reid, Annu. Rev. Phys. Chem. **54**, 397 (2003).
[42] A. E. Bragg, J. R. R. Verlet, A. Kammrath, O. Cheshnovsky, and D. M. Neumark, J. Chem. Phys. (to be published).
[43] H.-J. Flad, F. Schautz, Y. Wang, M. Dolg, and A. Savin, Eur. Phys. J. D **6**, 243 (1999).
[44] G. E. Moyano, R. Wesendrup, T. Söhnel, and P. Schwerdtfeger, Phys. Rev. Lett. **89**, 103401 (2002).
[45] I. Becker and O. Cheshnovsky, J. Chem. Phys. **110**, 6288 (1999).
[46] G. J. Martyna and B. J. Berne, J. Chem. Phys. **88**, 4516 (1988).
[47] G. J. Martyna and B. J. Berne, J. Chem. Phys. **90**, 3744 (1989).
[48] O. Cheshnovsky (Unpublished).
[49] P. Gerhardt, M. Niemietz, Y. D. Kim, and G. Gantefor, Chem. Phys. Lett. **382**, 454 (2003).
[50] M. Niemietz, P. Gerhardt, G. Gantefor, and Y. D. Kim, Chem. Phys. Lett. **380**, 99 (2003).